Research Article

Selective Growth of α-Al$_2$O$_3$ Nanowires and Nanobelts

Yong Zhang,[1] Ruying Li,[1] Xiaorong Zhou,[2] Mei Cai,[3] and Xueliang Sun[1]

[1] *Department of Mechanical and Materials Engineering, University of Western Ontario, London, Ontario, Canada N6A 5B9*
[2] *School of Materials, The University of Manchester, Manchester M60 1QD, UK*
[3] *Nanomaterials for Clean Energy Group, General Motors Research and Development Center, Warren, MI 48090-9055, USA*

Correspondence should be addressed to Xueliang Sun, xsun@eng.uwo.ca

We report the selective growth of α-Al$_2$O$_3$ nanowires and nanobelts via a catalyst-free chemical vapor deposition process under ambient pressure. By controlling the flow rates of the carrier gas, high-yield production of uniform alumina nanowires with diameter distribution (100 nm–200 nm) was achieved at a high growth rate over 200 μm/hour. Alumina nanobelts with variable width were also synthesized by modulating the carrier gas purge process. Further, the effects of temperatures and carrier gas flow rates on the growth of alumina nanostructures were also investigated. Oxygen partial pressure and supersaturation level of the aluminum suboxide are thought to be important factors in the formation process of the alumina nanowires or nanobelts. The typical growth of the alumina nanowires and nanobelts can be ascribed to vapor-solid (VS) mechanism.

1. INTRODUCTION

Recent progress in quasione dimensional (Q1D) nanostructured materials has gained increasing creditability of their advantages in both distinct properties and practical applications. Aside from nanotubes, the unique structural features of nanowires or nanobelts make them ideal candidates for both interconnects [1] and functional units [2, 3] in nanodevice integration. Metal oxide nanowires and nanobelts have attracted significant scientific interest due to their fascinating physical properties as well as their potential applications in optical [4], electronic [5, 6], optoelectronic [7, 8], piezoelectric [9], mechanical [10, 11], magnetic [12], chemical [13–16] sensors and nanodevices.

As a traditional structure material, aluminum oxide has featured excellent thermal stability and favorable mechanical properties. Thanks to peculiar properties recently explored in Q1D aluminum oxide, such as photoluminescence [17, 18], dielectric response [19], and selective catalysis [20]; keen interest has been aroused in probing new frontiers in this field. To date, crystalline and amorphous alumina nanowires, nanobelts, or nanorods have been synthesized through various techniques, including catalyst assisted [21–23] or catalyst free [18, 24, 25] chemical vapor deposition, chemical etching [26, 27], electrochemical deposition [28], arc-discharge [29], and surfactant-induced method [20]. As far as the catalyst-assisted growth of nanowires based on vapor-liquid-solid (VLS) growth mechanism, size of the nanowire diameter is well defined by the catalyst diameter. However, it still remains a big challenge of how to control the morphology and size of the Q1D alumina nanostructures via a catalyst-free method, which is essential to scale-up fabrication and industrial applications.

In this paper, we present a facile and effective way to selectively grow alumina nanowires or nanobelts under ambient pressure. This simple and controllable process promises scaled growth of the Q1D alumina nanostructures for potential industrial applications. The influence of experimental conditions, such as temperature and carrier gas flow rate, on the growth of alumina nanowires and nanobelts has been investigated. Further, the growth mechanism of the nanowires and nanobelts are discussed.

2. EXPERIMENTAL

A hot-wall chemical vapor deposition (HWCVD) system, with an alumina tube (2 inches outer diameter and 48 inches length) being mounted horizontally at the center, was employed in the present study. Q1D nanostructured alumina was fabricated under ambient pressure in such system with

reaction temperature and the flow rate of carrier gas being precisely controlled. Aluminum powder (A-547, 20 mesh, Fisher Scientific, Pa, USA), used as the starting material, was contained in an alumina boat and placed at the center of the alumina tube.

For the growth of alumina nanowires, high-purity argon gas (99.999%) was passed through the tube at a rate of 400 sccm (standard cubic centimeters per minute) for 30 minutes to purge air out of the furnace. Then, the furnace was heated to a target temperature ranging from 900°C–1350°C at a heating rate of 40°C/minute and maintained at the reaction temperature for 1 hour. Finally, the furnace was cooled down to room temperature at the end of the reaction. Argon gas was flown through the system at a controlled rate during the growth process.

Unlike the process for the growth of alumina nanowires, the gas purge step was skipped for the growth of alumina nanobelts. The furnace was directly heated to 1300°C at a heating rate of 40°C/minute, maintained at 1300°C for 1 hour, and then cooled down to room temperature. Again, argon gas was flown through the system at a controlled rate during the process.

The synthesized products were examined initially by using a Hitachi S-4500 field emission scanning electron microscopy (FESEM) equipped with energy dispersive X-ray (EDX) analysis facility. Further structural characterization of the Q1D nanostructures was carried out using a Rigaku-MiniFlex powder X-ray diffraction spectrometer (XRD), a JEOL 2010 transmission electron microscope (TEM), and a Tecnai G^2 F30 high-resolution transmission electron microscope (HRTEM).

3. RESULTS AND DISCUSSION

3.1. Morphological and structural characterization

For the nanowires synthesis, when the reaction temperature was above 1100°C, white cotton-wool-like products could be collected from inner wall of the alumina boat. In this case, the residue aluminum/aluminum oxide solidified into a single molten block after heating at the temperature higher than 1100°C. However, when the reaction temperature was below 1100°C, no such products could be harvested from the alumina boat. Therefore, the residual aluminum particles were collected for characterization. In this case, the particle size becomes much bigger due to melting and solidification after reaction.

Figure 1 shows scanning electron micrographs of the products obtained at various reaction temperatures. Short nanorods, 5–10 μm in length and 0.5–1 μm in diameter, were observed on the surface of residual aluminum particle for the reaction temperature of 900°C, as shown in Figure 1(a). Thinner nanorods, of 200–300 nm in diameter, mixed with some nanosheets (indicated by arrow), were generated on the surface of the residual aluminum particles at the reaction temperature of 1000°C (see Figure 1(b)). When the temperature was increased to 1100°C, cotton-wool-like products were formed on inner wall of the alumina boat. A scanning electron micrograph of such product

is shown in Figure 1(c), revealing nanowires of 100 nm–1μm in diameter. For the reaction temperature of 1300°C, the scanning electron micrograph of Figure 1(d) shows nanowires with uniform diameter of 200–400 nm. EDX analysis of the nanowires gave yields of aluminum and oxygen, indicating the formation of alumina nanostructures. Further, when the reaction temperature was above 1350°C, the nanowires tended to become thick and nonuniform in diameter. Therefore, the size dependence of the nanowires on argon gas flow rate was further investigated by fixing reaction temperature at 1300°C, as described in the following paragraph.

Scanning electron micrographs of alumina nanostructures grown at 1300°C under different argon gas flow rates are shown in Figure 2. With argon gas flow rate in the range of 40–100 sccm, the diameter of the alumina nanowires ranges from 200 to 800 nm (see Figures 2(a) and 2(b)). Interestingly, it was observed that increased argon gas flow rates favored the growth of thinner alumina nanowires. Neat alumina nanowires with diameter distribution of 200–400 nm and 100–200 nm were produced at the argon gas flow rate of 200 sccm and 600 sccm, respectively, (see Figures 2(c) and 2(d)). Further increase in argon gas flow rate to above 600 sccm showed little influence on the morphology and diameter of the nanowires.

Further characterization of the nanostructures was carried out using transmission electron microscopy and X-ray diffraction spectrometer, as shown in Figure 3. The bright field TEM image reveals that the nanowires are uniform and neat, with the diameter of about 100 nm as shown in Figure 3(a). Figure 3(b) displays XRD pattern of the product, which can be assigned to rhombohedral structure of α-Al$_2$O$_3$. HRTEM lattice image of the nanowire in Figure 3(c) indicates that the lattice spacing is around 0.43 nm, corresponding to {003} set of planes of α-Al$_2$O$_3$. As shown in Figure 3(d), the selected area electron diffraction (SAED) pattern can be fully indexed as rhombohedral structure of α-Al$_2$O$_3$. By recording the SAED pattern along the nanowires, it is evident that each individual α-Al$_2$O$_3$ nanowire is a single crystal.

Interestingly, it was found that careful control of argon gas purge process could also modulate the morphology of alumina nanostructures. As shown in Figures 1 and 2, nanowires were produced when a thirty-minute argon gas purge step was applied. However, under the same synthesis conditions, but with the argon purge step being skipped, nanostructures of completely different morphologies were produced, as shown in Figure 4. At the argon gas flow rate of 40 sccm, only thick nanorods with very rough surface were generated (see Figure 4(a)). Thin nanobelts, with the widths ranging from 200 nm to a couple of micrometers, were obtained with an increased argon flow rate ranging from 150 sccm to 350 sccm (see Figures 4(b) and 4(c)). When an argon gas flow rate of 600 sccm was applied, a mixture of nanobelts and nanowires was produced (see Figure 4(d)), which is similar to the observation in Figure 1(d). Figure 5 shows increased magnification XRD, SEM, and TEM images of typical alumina nanobelts obtained at 1300°C at an argon gas flow rate of 150 sccm. The nanobelts are approximately
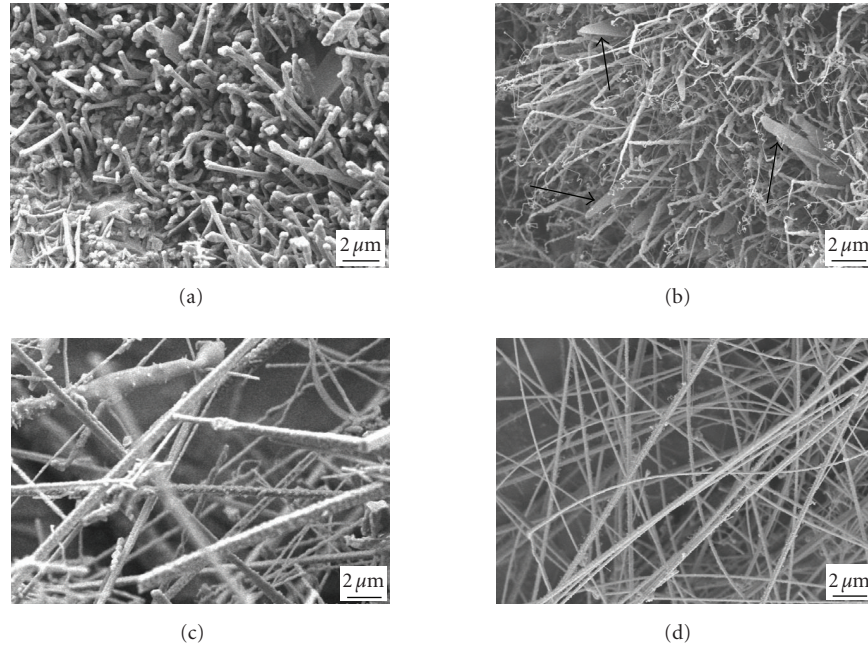
(a)

(b)

(c)

(d)

FIGURE 1: FESEM images show alumina nanowires synthesized under different temperatures with 200 sccm argon gas. (a) 900°C, (b) 1000°C, (c) 1100°C, (d) 1300°C.
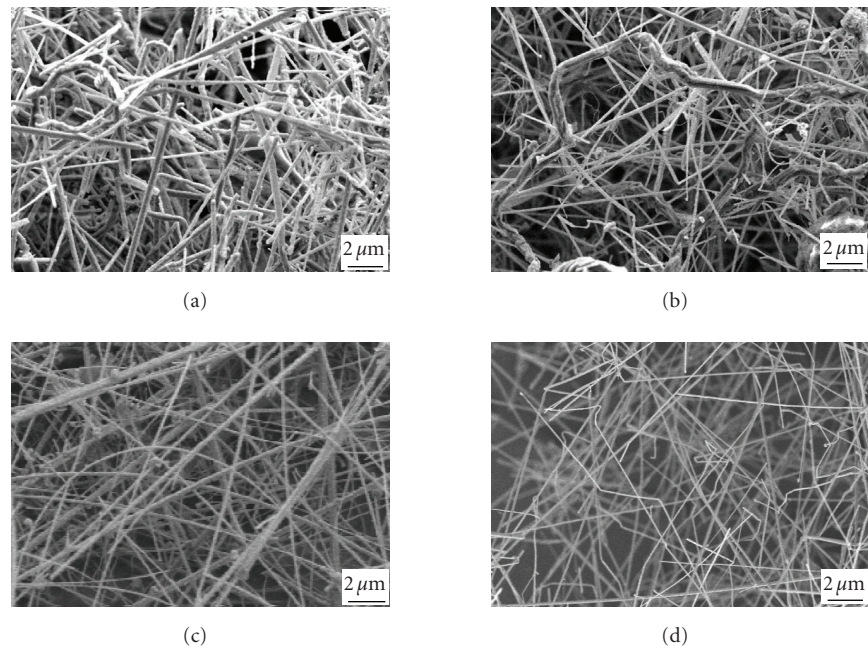

(a)

(b)

(c)

(d)

FIGURE 2: FESEM images show alumina nanowires synthesized at 1300°C under different argon gas flow rates. (a) 40 sccm, (b) 100 sccm, (c) 200 sccm, and (d) 600 sccm.

500 nm wide and a few tens nanometer thick. The XRD pattern and selected area diffraction pattern confirm that the nanobelts are α-Al_2O_3 with the rhombohedral structure.

3.2. Growth mechanism

For catalyst-assisted growth of alumina and many semi-conductor nanowires, the vapor-liquid-solid (VLS) growth mechanism has been widely accepted [23, 30]. The presence of solidified spherical droplets at the tips of nanowires or others is commonly considered to be evidence of the VLS mechanism. The growth process can be divided into two stages: the nucleation and growth of eutectic alloy droplets and the growth of nanowires through the liquid droplets due to supersaturation. However, no catalyst particles were observed at the tips of the nanowires or nanobelts through
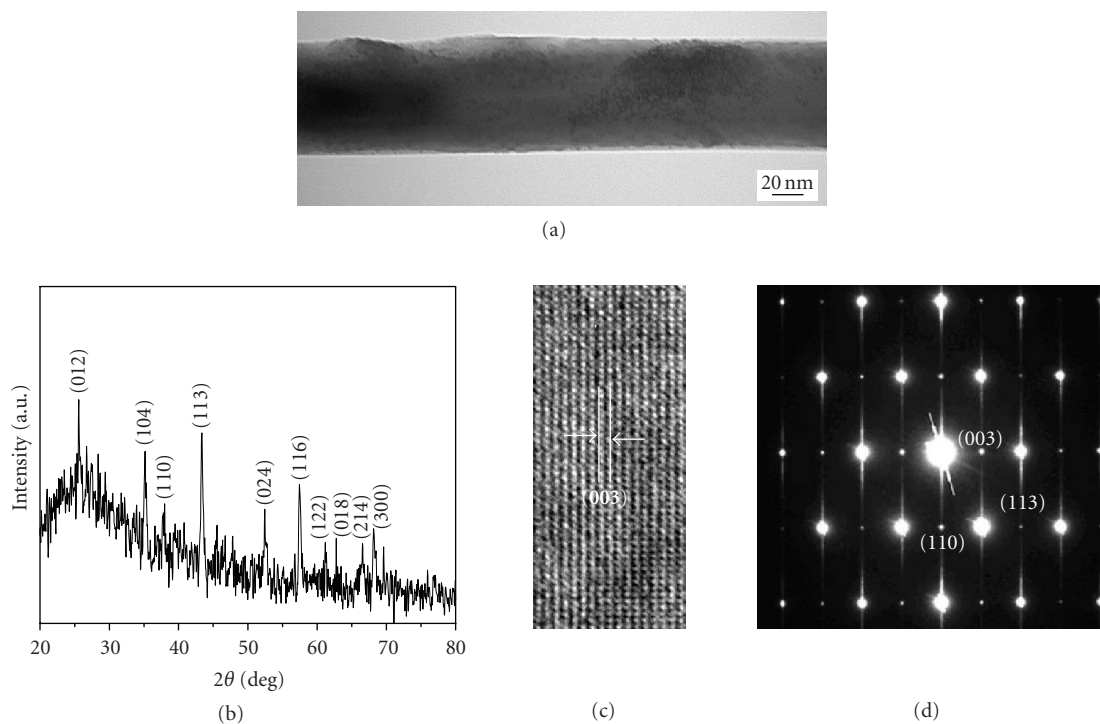
(a)

(b)

(c)

(d)

FIGURE 3: (a) Bright field image, (b) XRD pattern, (c) HRTEM image, and (d) SAED pattern of the Al_2O_3 nanowire.
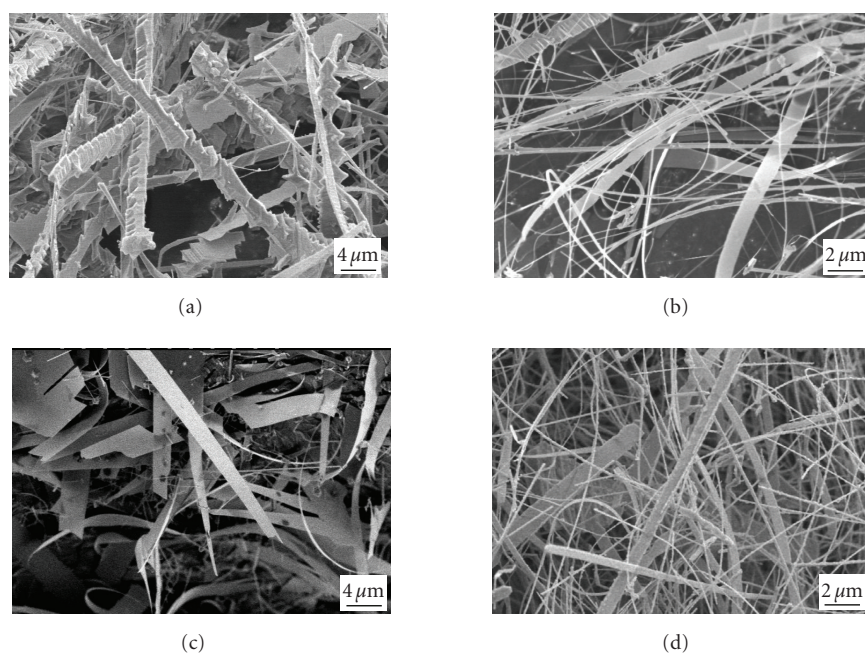

(a)

(b)

(c)

(d)

FIGURE 4: FESEM images show alumina nanobelts obtained at 1300°C under different argon gas flow rates. (a) 40 sccm, (b) 150 sccm, (c) 350 sccm, and (d) 600 sccm.

SEM and TEM investigations in our experiments, indicating that the growth of alumina nanowires or nanobelts is not governed by the VLS growth mechanism in the present study. In our experiment, an alumina boat was used as a container for the aluminum powder. It was observed that the alumina boat under aluminum powder was partly dissolved during synthesis process. The degree of such dissolution was dependent on the temperature employed. This indicates an occurrence of interaction between the alumina boat and the aluminum powder during the synthesis process. In order to
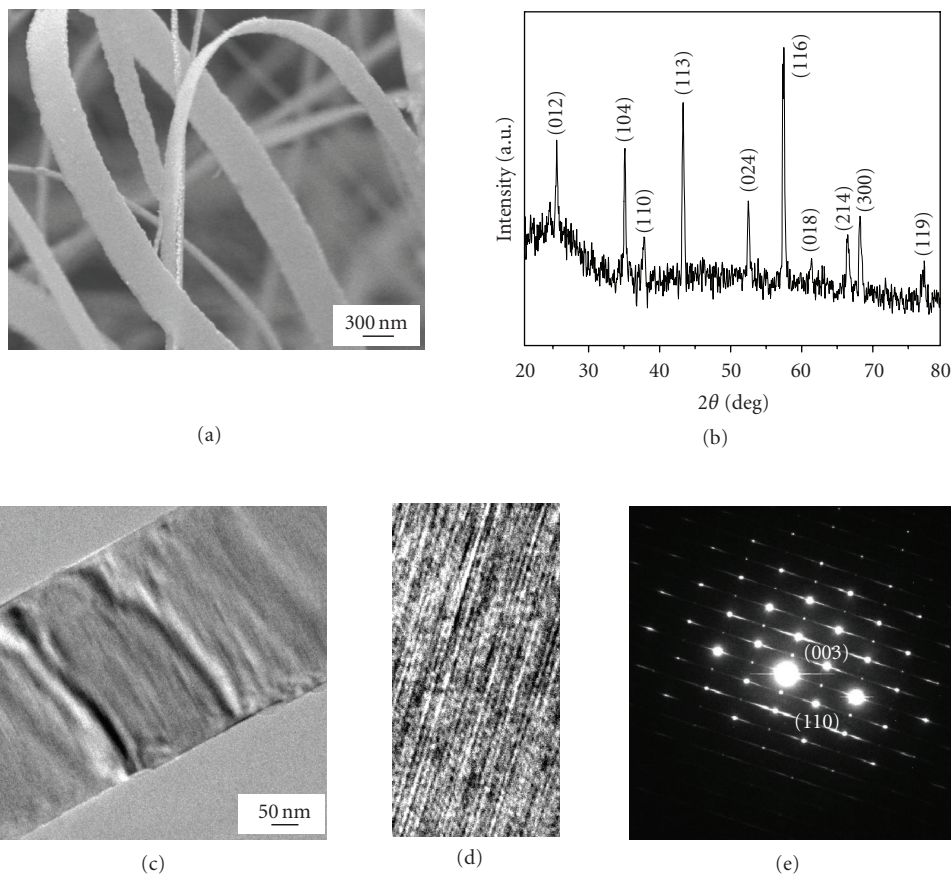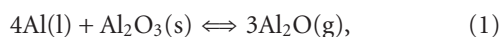
(a)

(b)

(c)

(d)

(e)

FIGURE 5: (a) High magnification FESEM image, (b) XRD of the Al$_2$O$_3$ nanobelts, (c) TEM image, (d) HRTEM image, and (e) the corresponding SAED pattern of a typical Al$_2$O$_3$ nanobelt.

identify the role of alumina in the reaction process, we used a mixture of metallic aluminum and alumina powder to take the place of sole metal aluminum powder as the starting material. While a certain amount of alumina powder was used, the structure of the products was similar to the case without using the alumina powder, and the alumina boat was almost not etched. The results indicate that: (1) the alumina boat which has a similar role to an alumina plate was involved into the reaction for growing the nanowires or nanobelts; (2) the alumina source for the product growth can be supplied by extra added alumina powders or plates.

For Al–Al$_2$O$_3$ system, various aluminum-containing vapor species, including Al, AlO, Al$_2$O, and Al$_2$O$_2$ [31], are generated at the temperatures employed in the present study. Such species may be involved in the synthesis of alumina nanostructured materials. From a vapor pressure study of aluminum-oxygen system reported by Brewer and Searcy [31], Al and Al$_2$O are the principal vapor components under reducing (Al–Al$_2$O$_3$) conditions.

Therefore, it is postulated that the formation of the alumina nanowires or nanobelts is based on the following reactions and phase transition:

$$4\text{Al}(l) + \text{Al}_2\text{O}_3(s) \Longleftrightarrow 3\text{Al}_2\text{O}(g), \tag{1}$$

$$\text{Al}_2\text{O}(g) + \text{O}_2(g) \Longleftrightarrow \text{Al}_2\text{O}_3(s), \tag{2}$$

$$4\text{Al}(l) + 3\text{O}_2(g) \Longleftrightarrow 2\text{Al}_2\text{O}_3(s), \tag{3}$$

$$4\text{Al}(g) + 3\text{O}_2(g) \Longleftrightarrow 2\text{Al}_2\text{O}_3(s). \tag{4}$$

It is known aluminum suboxide (Al$_2$O) is thermodynamically stable between 1050°C and 1600°C [32]. At the temperature above 1100°C, aluminum reacts with the alumina boat and generates Al$_2$O vapor as reaction (1). There are two available alumina sources here: one is the reaction product between aluminum and trace amount of oxygen in the carrier gas or from air leakage or residue oxygen in the reaction tube, and the other is the alumina boat. When the supersaturation of the reactant vapors increases to a level at which nuclei formed, the combination of Al$_2$O vapor and oxygen inside the chamber can produce nanosized alumina nuclei attached on the inner wall of the alumina boat which provides preferential nucleation sites for the alumina nanowire growth. Finally, alumina nanowires or nanobelts are formed as shown in reaction (2) through a process of diffusion, collision of atoms, and reaction between the vapor molecules (including Al$_2$O vapor and O$_2$ in this experiment), which follows a vapor-solid (VS) growth mechanism. In this case, the growth of the nanowires/nanobelts can be mainly attributed from the result of reactions (1) and (2).

While the temperature is in the range of 900°C–1000°C, no products could be collected from the inner wall of

the alumina boat. In this case, alumina nanorods and nanosheets were observed on the surface of the residual aluminum particles (see Figures 1(a) and 1(b)). Within this temperature range, Al_2O vapor is metastable. In this case, the nucleation and growth of the alumina nanostructures may be more dependent on the reactions between the aluminum liquid/vapor and the oxygen inside or close to the molten aluminum surface as shown in reactions (3) and (4). The reactions can produce tiny alumina nuclei in the molten aluminum. Due to poor wettability of molten aluminum with alumina nuclei [33], high surface tension of the molten aluminum drives the alumina nuclei to the molten aluminum surface and prevents the nuclei from aggregation, which favors the preferetial growth of the alumina perpendicular to the molten aluminum surface. The subsequent growth of surface nuclei could occur through attachment kinetics with the reactant species in the dissolved phase as illustrated in reaction (3) or with gas-phase species as illustrated in reaction (4).

With decreasing temperature (below 900°C), too low temperature probably is not able to induce the growth of alumina in quasi one dimension. The alumina obtained could coalesce on the molten surface to form a crust and result in a thick film over molten aluminum.

Another interesting question is why the nanowires and nanobelts can be selectively grown. Song et al. have reported that the partial pressure of oxygen plays a key role in determining the morphology of the Q1D ZnO nanostructures by VLS growth mode under vacuum conditions, in which Q1D anisotropic growth of ZnO nanowires was promoted by controllably decreasing oxygen pressure in the reaction chamber [34]. On the other hand, Ye et al. have suggested that the nonequilibrium kinetic growth caused by high supersaturation level may allow the formation of a low-surface-energy tip, which favors two-dimensional growth of the nanostructures [35]. Park et al. have reported that transformation from Q1D growth of ZnO nanowires to Q2D growth of ZnO nanobelts occurred with increasing supersaturation level of the reactant vapors governed by VS growth [36]. According to Dalal et al. and Lee et al.'s reports, higher oxygen partial pressure has been proposed as an important factor in generating ZnO [37] and Ga_2O_3 nanobelts [38], respectively, in comparison with the nanowire growth.

In our case, we propose that purge process can produce low partial pressure of oxygen inside the chamber though the condition of air leakage, and residue oxygen still needs to be considered, while skipping the purge process not only keeps a high oxygen partial pressure but also may trigger a generation of high supersaturation level of aluminum suboxide vapor during the heating process as illustrated in the reactions (3), (4), and (1) due to high oxygen content. So we intend to attribute the growth of the Al_2O_3 nanowires to the low oxygen partial pressure, and the growth of the Al_2O_3 nanobelts to the combination effect of excessive supersaturation level of the aluminum suboxide vapor and high oxygen partial pressure in the synthesis process.

In the experiments, there are probably three sources which provide the oxygen in the synthesis of the Q1D alumina nanostructures: (1) the argon gas (99.999% purity),
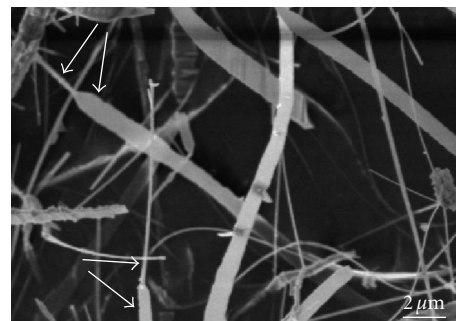
(a)

(b)

FIGURE 6: (a) SEM image of the Al_2O_3 nanobelts showing the transition between the nanobelt and nanowire, (b) TEM image of a single Al_2O_3 nanobelt revealing the transition from belt-like to wire-like structure.

which contains a small amount of oxygen with the partial pressure of 10^{-5} atm [39], (2) residue oxygen in the reaction chamber after the purge, (3) air leakage. Similar to the case that Park et al. discussed [40], low oxygen partial pressure favors one-dimensional growth of the products. After the purge process, most of the oxygen was excluded from the chamber. However, the oxygen supply coming from air leakage and residue oxygen inside the chamber were not able to be effectively restrained by the argon gas while a low flow rate of argon was applied in the growth process. With increasing argon flow rate, oxygen partial pressure inside the chamber decreased, and gradually closed to the internal oxygen partial pressure of the argon gas. This may be one of the reasons why higher argon flow rate favored the growth of thinner alumina nanowires. While Ar purge process was not conducted, oxygen partial pressure inside the alumina tube kept the same as ambient environment before heating. The furnace was then heated as soon as Ar gas was introduced. In this circumstance, oxygen partial pressure decreased inside the alumina tube while temperature of the furnace increased over the time. On the other hand, high supersaturation level of aluminum suboxide might be triggered during the heating process due to high oxygen content inside the chamber. Depending on the supersaturation level of aluminum suboxide and oxygen partial pressure at the target temperature, alumina nanostructures with different morphologies were obtained. At a lower Ar flow rate, the oxygen partial pressure remained very high, and excessive supersaturation level of the aluminum suboxide was generated when the target temperature was achieved, allowing quick growth perpendicular to the longitudinal axis of the product. Therefore, thick column-like structure was produced (see Figure 4(a)). Proper argon flow rates might activate secondary growth sites and heterogeneous

nucleation on the side of the Q1D structures. This in turn resulted in Q2D growth of the structures and thus alumina nanobelts were obtained (see Figures 4(b) and 4(c)). While Ar flow rate was further increased, the oxygen partial pressure and supersaturation level of aluminum suboxide became relative low at the target temperature, which is similar to the nanowire growth that discussed above. Therefore, both nanowires and nanobelts can be observed as shown in Figure 4(d). For the growth of the nanobelts, a question may arise, to what extent the effect of the nonpurge measure can last for growing the nanobelts because the oxygen partial pressure decreases continuously with increasing growth time. Figure 6(a) shows a typical SEM image of the nanobelts (from the same sample as shown in Figure 4(b)). As marked by the white arrows, a morphological transition from the nanobelt to nanowire is observed. It reveals that the growth of the nanobelt ends with a wire-like morphology due to decreasing oxygen partial pressure and supersaturation level of the aluminum suboxide. This indicates that the growth of the nanobelts is time-dependent and needs to be carefully designed. Figure 6(b) shows a typical TEM image of the nanobelt/nanowire structure at the wire-like end. No catalyst particle is observed at the tip of the nanowire, which conforms to the VS growth model. The arrow in Figure 6(b) reveals the growth direction of the product.

Further investigation of other processing parameters and precise control of oxygen partial pressure that affect the morphology of nanostructures generated in Al–Al$_2$O$_3$ system is currently being undertaken in our group.

4. CONCLUSIONS

We have demonstrated a facile and cost effective way to selective synthesis of high yield uniform α-Al$_2$O$_3$ nanowires and nanobelts. This catalyst and vacuum free method is promising in high throughout production of quasi one-dimensional nanostructured alumina. The typical growth of the nanowires and nanobelts can be ascribed to vapor-solid (VS) mechanism. It is suggested that oxygen partial pressure and supersaturation level of the aluminum suboxide play important roles in determining morphology of the nanostructures. A lower oxygen partial pressure favors the formation of alumina nanowires, while the combination effect of a relatively higher oxygen pressure and high supersaturation level of the aluminum suboxide results in the growth of alumina nanobelts. Such precise control over morphologies makes it possible for potential industrial applications of nanostructured Al$_2$O$_3$ materials.

ACKNOWLEDGMENTS

REFERENCES

[1] R. He, D. Gao, R. Fan, et al., "Si nanowire bridges in microtrenches: integration of growth into device fabrication," *Advanced Materials*, vol. 17, no. 17, pp. 2098–2102, 2005.

[2] Y. Xia, P. Yang, Y. Sun, et al., "One-dimensional nanostructures: synthesis, characterization, and applications," *Advanced Materials*, vol. 15, no. 5, pp. 353–389, 2003.

[3] B. K. Teo and X. H. Sun, "Silicon-based low-dimensional nanomaterials and nanodevices," *Chemical Reviews*, vol. 107, no. 5, pp. 1454–1532, 2007.

[4] A. M. Glushenkov, H. Z. Zhang, J. Zou, G. Q. Lu, and Y. Chen, "Efficient production of ZnO nanowires by a ball milling and annealing method," *Nanotechnology*, vol. 18, no. 17, Article ID 175604, 6 pages, 2007.

[5] P. Nguyen, H. T. Ng, T. Yamada, et al., "Direct integration of metal oxide nanowire in vertical field-effect transistor," *Nano Letters*, vol. 4, no. 4, pp. 651–657, 2004.

[6] W. I. Park, J. S. Kim, G.-C. Yi, and H.-J. Lee, "ZnO nanorod logic circuits," *Advanced Materials*, vol. 17, no. 11, pp. 1393–1397, 2005.

[7] M. Law, L. E. Greene, J. C. Johnson, R. Saykally, and P. Yang, "Nanowire dye-sensitized solar cells," *Nature Materials*, vol. 4, no. 6, pp. 455–459, 2005.

[8] W. I. Park and G.-C. Yi, "Electroluminescence in n-ZnO nanorod arrays vertically grown on p-GaN," *Advanced Materials*, vol. 16, no. 1, pp. 87–90, 2004.

[9] Z. L. Wang and J. Song, "Piezoelectric nanogenerators based on zinc oxide nanowire arrays," *Science*, vol. 312, no. 5771, pp. 242–246, 2006.

[10] T. Ikuno, S.-I. Honda, T. Yasuda, et al., "Thermally driven nanomechanical deflection of hybrid nanowires," *Applied Physics Letters*, vol. 87, no. 21, Article ID 213104, 3 pages, 2005.

[11] M.-F. Yu, M. Z. Atashbar, and X. Chen, "Mechanical and electrical characterization of β-Ga$_2$O$_3$ nanostructures for sensing applications," *IEEE Sensors Journal*, vol. 5, no. 1, pp. 20–25, 2005.

[12] T. Zhang, C. Jin, J. Zhang, X. Lu, T. Qian, and X. Li, "Microstructure and magnetic properties of ordered La$_{0.62}$Pb$_{0.38}$MnO$_3$ nanowire arrays," *Nanotechnology*, vol. 16, no. 11, pp. 2743–2747, 2005.

[13] K. T. Nam, D.-W. Kim, P. J. Yoo, et al., "Virus-enabled synthesis and assembly of nanowires for lithium ion battery electrodes," *Science*, vol. 312, no. 5775, pp. 885–888, 2006.

[14] J. Polleux, A. Gurlo, N. Barsan, U. Weimar, M. Antonietti, and M. Niederberger, "Template-free synthesis and assembly of single-crystalline tungsten oxide nanowires and their gas-sensing properties," *Angewandte Chemie International Edition*, vol. 45, no. 2, pp. 261–265, 2005.

[15] A. Kolmakov, Y. Zhang, G. Cheng, and M. Moskovits, "Detection of CO and O$_2$ using tin oxide nanowire sensors," *Advanced Materials*, vol. 15, no. 12, pp. 997–1000, 2003.

[16] V. V. Sysoev, B. K. Button, K. Wepsiec, S. Dmitriev, and A. Kolmakov, "Toward the nanoscopic "electronic nose": hydrogen vs carbon monoxide discrimination with an array of individual metal oxide nano- and mesowire sensors," *Nano Letters*, vol. 6, no. 8, pp. 1584–1588, 2006.

[17] T. Li, S. Yang, and Y. Du, "Strongly luminescent Cr-doped alumina nanofibres," *Nanotechnology*, vol. 16, no. 4, pp. 365–368, 2005.

[18] X.-S. Fang, C.-H. Ye, X. S. Peng, Y. H. Wang, Y. C. Wu, and L.-D. Zhang, "Temperature-controlled growth of α-Al$_2$O$_3$ nanobelts and nanosheets," *Journal of Materials Chemistry*, vol. 13, no. 12, pp. 3040–3043, 2003.

[19] X.-S. Fang, C.-H. Ye, L.-D. Zhang, and T. Xie, "Twinning-mediated growth of Al_2O_3 nanobelts and their enhanced dielectric responses," *Advanced Materials*, vol. 17, no. 13, pp. 1661–1665, 2005.

[20] H. Y. Zhu, J. D. Riches, and J. C. Barry, "γ-alumina nanofibers prepared from aluminum hydrate with poly(ethylene oxide) surfactant," *Chemistry of Materials*, vol. 14, no. 5, pp. 2086–2093, 2002.

[21] Y. Z. Jin, Y. Q. Zhu, K. Brigatti, H. W. Kroto, and D. R. M. Walton, "Catalysed growth of novel aluminium oxide nanorods," *Applied Physics A*, vol. 77, no. 1, pp. 113–115, 2003.

[22] N.-F. Wu, H.-J. Chen, Y.-L. Chueh, S.-J. Lin, L.-J. Chou, and W.-K. Hsu, "Doped spiral alumina nanowires," *Chemical Communications*, no. 2, pp. 204–206, 2005.

[23] C. C. Tang, S. S. Fan, P. Li, M. Lamy de la Chapelle, and H. Y. Dang, "In situ catalytic growth of Al_2O_3 and Si nanowires," *Journal of Crystal Growth*, vol. 224, no. 1-2, pp. 117–121, 2001.

[24] X. S. Peng, L.-D. Zhang, G.-W. Meng, et al., "Photoluminescence and infrared properties of α-Al_2O_3 nanowires and nanobelts," *Journal of Physical Chemistry B*, vol. 106, no. 43, pp. 11163–11167, 2002.

[25] Q. Zhao, X. Xu, H. Zhang, Y. Chen, J. Xu, and D. Yu, "Catalyst-free growth of single-crystalline alumina nanowire arrays," *Applied Physics A*, vol. 79, no. 7, pp. 1721–1724, 2004.

[26] Z. L. Xiao, C. Y. Han, U. Welp, et al., "Fabrication of alumina nanotubes and nanowires by etching porous alumina membranes," *Nano Letters*, vol. 2, no. 11, pp. 1293–1297, 2002.

[27] Y. T. Tian, G.-W. Meng, T. Gao, et al., "Alumina nanowire arrays standing on a porous anodic alumina membrane," *Nanotechnology*, vol. 15, no. 1, pp. 189–191, 2004.

[28] Y.-T. Pang, G.-W. Meng, L.-D. Zhang, et al., "Electrochemical synthesis of ordered alumina nanowire arrays," *Journal of Solid State Electrochemistry*, vol. 7, no. 6, pp. 344–347, 2003.

[29] W. F. Li, X. L. Ma, W. S. Zhang, W. Zhang, Y. Li, and Z. D. Zhang, "Synthesis and characterization of γ-Al_2O_3 nanorods," *Physica Status Solidi (A)*, vol. 203, no. 2, pp. 294–299, 2006.

[30] P. Yang, H. Yan, S. Mao, et al., "Controlled growth of ZnO nanowires and their optical properties," *Advanced Functional Materials*, vol. 12, no. 5, pp. 323–331, 2002.

[31] L. Brewer and A. W. Searcy, "The gaseous species of the Al-Al_2O_3 system," *Journal of the American Chemical Society*, vol. 73, no. 11, pp. 5308–5314, 1951.

[32] M. Hoch and H. L. Johnston, "Formation, stability and crystal structure of the solid aluminum suboxides: Al_2O and AlO," *Journal of the American Chemical Society*, vol. 76, no. 9, pp. 2560–2561, 1954.

[33] S. Sharma and M. K. Sunkara, "Direct synthesis of gallium oxide tubes, nanowires, and nanopaintbrushes," *Journal of the American Chemical Society*, vol. 124, no. 41, pp. 12288–12293, 2002.

[34] J. Song, X. Wang, E. Riedo, and Z. L. Wang, "Systematic study on experimental conditions for large-scale growth of aligned ZnO nanwires on nitrides," *Journal of Physical Chemistry B*, vol. 109, no. 20, pp. 9869–9872, 2005.

[35] C. H. Ye, X.-S. Fang, Y. Hao, X. Teng, and L.-D. Zhang, "Zinc oxide nanostructures: morphology derivation and evolution," *Journal of Physical Chemistry B*, vol. 109, no. 42, pp. 19758–19765, 2005.

[36] J.-H. Park, H.-J. Choi, Y.-J. Choi, S.-H. Sohn, and J.-G. Park, "Ultrawide ZnO nanosheets," *Journal of Materials Chemistry*, vol. 14, no. 1, pp. 35–36, 2004.

[37] S. H. Dalal, D. L. Baptista, K. B. K. Teo, R. G. Lacerda, D. A. Jefferson, and W. I. Milne, "Controllable growth of vertically aligned zinc oxide nanowires using vapour deposition," *Nanotechnology*, vol. 17, no. 19, pp. 4811–4818, 2006.

[38] J.-S. Lee, K. Park, S. Nahm, S.-W. Kim, and S. Kim, "Ga_2O_3 nanomaterials synthesized from ball-milled GaN powders," *Journal of Crystal Growth*, vol. 244, no. 3-4, pp. 287–295, 2002.

[39] F.-H. Lu and H.-Y. Chen, "XPS analyses of TiN films on Cu substrates after annealing in the controlled atmosphere," *Thin Solid Films*, vol. 355-356, pp. 374–379, 1999.

[40] J.-H. Park, Y.-J. Choi, and J.-G. Park, "Synthesis of ZnO nanowires and nanosheets by an O_2-assisted carbothermal reduction process," *Journal of Crystal Growth*, vol. 280, no. 1-2, pp. 161–167, 2005.